catalysts

MDPI

Article

The Improvement of Coralline-Like $ZnGa_2O_4$ by Cocatalysts for the Photocatalytic Degradation of Rhodamine B

Jia Yang *, Xiaorui Sun *, Wanxi Yang, Meixia Zhu and Jianwei Shi

Chongqing Key Laboratory of Inorganic Special Functional Materials, College of Chemistry and Chemical Engineering, Yangtze Normal University, Fuling, Chongqing 408100, China; yangwanxi@163.com (W.Y.); zhumeixia@163.com (M.Z.); shijianwei@163.com (J.S.)

* Correspondence: yangjiayznu@163.com (J.Y.); sunxiaoruiyznu@163.com (X.S.); Tel.: +86-18716372096 (J.Y.); +86-18883876787 (X.S.)

Received: 3 January 2020; Accepted: 9 February 2020; Published: 11 February 2020

Abstract: To date, various methods have been used to synthesize $ZnGa_2O_4$ material to promote photodegradation performance. However, cocatalysts, which usually play a crucial role in the photocatalyst system, have not been studied extensively in photocatalytic degradation reactions. In this paper, $ZnGa_2O_4$ semiconducting material was synthesized by a traditional high-temperature solid-state reaction. The as-prepared powder was characterized by X-ray diffraction (XRD), scanning electron microscopy (SEM), and ultraviolet–visible diffused reflectance spectroscopy. The results indicate that the as-prepared sample is a highly crystallized granular sample with a bandgap of 4.44 eV and a uniform particle size distribution. Density functional theory (DFT) was utilized to calculate the electronic structure of $ZnGa_2O_4$. The valence bands and conduction bands were chiefly composed of O 2p atomic orbitals and the hybridization orbitals of Ga 4s4p and Zn4s4p, respectively. The photocatalytic performance was tested via the decomposition of rhodamine B (RhB) under the irradiation of ultraviolet light. Cu, Ag, Au, Ni, Pt, and Pd cocatalysts were loaded on the $ZnGa_2O_4$ photocatalyst by a photodeposition method. The relatively optimal cocatalyst of $ZnGa_2O_4$ in the photocatalytic degradation reaction is Au. Thereafter, the effect of loading different usage amounts of the Au cocatalyst for the photodegradation of the $ZnGa_2O_4$ photocatalyst was studied in detail. The experimental results displayed that the optimum photodegradation activity was confirmed with the 3 wt% Au/$ZnGa_2O_4$ sample, which was 14.1 times more than the unloaded photocatalyst. The maximum photocatalytic degradation ratio of RhB was 96.7%, with 180 min under ultraviolet light.

Keywords: photocatalysis; cocatalyst; zinc gallate; rhodamine B

1. Introduction

$ZnGa_2O_4$ with its spinel structure is an important P-block semiconducting material and has extensive application prospects in flat panel displays, vacuum fluorescent displays, day-blind detectors, fluorescent materials, and photocatalytic materials [1–5]. Because of its excellent performance, $ZnGa_2O_4$ has been widely investigated in the photocatalytic field, e.g., water splitting under ultraviolet light illumination [6], photocatalytic hydrogen production [7], photocatalytic reduction of CO_2 [8], the reduction of heavy metal ions via photocatalytic reaction [9], the photocatalytic oxidation reaction of organic compounds [10], and the photodegradation of dyes [11–13]. Especially for the photodecomposition of various dyes, including methylene blue (MB), methyl orange, and rhodamine B (RhB), are utilized as a model pollutant to test the photocatalytic performance of $ZnGa_2O_4$ photocatalyst. This is due to the large bandgap width possessed by $ZnGa_2O_4$, which is reported to be 4.5 eV in the

literature [14]. Hence, it has a high conduction band potential, which is conducive to the generation of hydroxyl radicals or superoxide anions for photocatalytic degradation.

In order to enhance the photocatalytic performance of $ZnGa_2O_4$, the reported experimental results focus on utilizing a variety of synthesis methods to control the morphology of $ZnGa_2O_4$ samples. For example, $ZnGa_2O_4$ powder and film materials were prepared by the sol–gel method, and their photocatalytic degradation of MB was studied [15]. $ZnGa_2O_4$ powder material was prepared by a hydrothermal reaction. The morphology of the material was controlled by the dosage of surfactant, the reaction temperature, and the reaction time, and the photocatalytic oxidation of RhB was studied over the material [16]. A "rice-like" $ZnGa_2O_4$ sample was prepared by controlling the pH value via a hydrothermal reaction with a template. Compared to the photocatalyst that was synthesized by high-temperature solid-state reaction, the photocatalytic activity was greatly improved [9]. Nanoparticles with uniform morphology were obtained via microwave hydrothermal reaction to achieve efficient degradation of dyes [17]. Nanocrystalline samples with exposed {111} and {110} crystal surfaces were fabricated by a hydrothermal method to enhance photocatalytic hydrogen production [7]. A double-layer spherical powder material was obtained via a hydrothermal reaction, and its photocatalytic reduction performance on carbon dioxide was studied [8]. To promote the photocatalytic activity of $ZnGa_2O_4$, a single crystal with octahedral shape [18] was obtained by a chemical gas phase transport method, and photonic crystals were prepared as well [19]. Different synthetic methods were used to synthesize materials with different morphologies to improve the photocatalytic hydrogen evolution of a $ZnGa_2O_4$ sample [5]. In fact, in addition to the important influence of morphology on the photocatalytic performance, a cocatalyst usually plays a crucial role in photocatalytic materials [20,21]. Recently, Ag, Pt, and Ru catalysts were loaded on $ZnGa_2O_4$ to enhance the photocatalytic reduction activity of CO_2 [22]. However, there has been no systematic research on the impact of cocatalysts on the photodegradation activity. Therefore, it is of great significance to study the loading of catalysts based on $ZnGa_2O_4$ photocatalytic material.

In this paper, a $ZnGa_2O_4$ model photocatalyst was obtained by a traditional high-temperature solid-state method. Various Cu, Ag, Au, Ni, Pd, and Pt cocatalysts were loaded on the $ZnGa_2O_4$ model photocatalyst via a photodeposition method. The photocatalytic activity of the decomposition of RhB was tested. The photocatalytic results were quantificationally analyzed by the rate constant of the first-order kinetics model. In addition, to comprehend the mechanism of the photocatalytic process of the reaction, the energy band structure of $ZnGa_2O_4$ was calculated by the plane-wave pseudopotential method.

2. Results and Discussion

Figure 1 displays the X-ray diffraction (XRD) pattern of $ZnGa_2O_4$, which was synthesized by a high-temperature solid-state reaction. Compared to the simulated XRD pattern (ICSD-81113), the as-prepared sample is pure phase without any impurity. The XRD peaks of the $ZnGa_2O_4$ sample were further identified by TOPAS software (see Figure S1). The space group is *Fd-3m*, and the cell parameter and cell volume are a = 8.331 Å and V = 111.9 Å^3, respectively. The sharp peaks reveal the high crystallinity of the as-prepared semiconducting material. The medial crystallite size of $ZnGa_2O_4$ was computed via Scherrer's formula: $d = K\gamma/B\cos\theta_B$, in which d is the crystallite size of the assumed spherical particle, K = 0.9, γ is the wavelength of X-ray radiation, and B and θ_B are the full width at half-maximum and diffraction angle of the diffracted peak, respectively [23]. The estimated crystallite size based on the (311) peak for $ZnGa_2O_4$ is approximately 74.2 nm.

Figure 2a presents a scanning electron microscope (SEM) image of the $ZnGa_2O_4$ sample; it shows uniform morphology in the large-scale zone, which indicates that this sample is pure. Figure 2b displays an SEM image of the $ZnGa_2O_4$ sample, which is a nanosized particle, 40–120 nm. The smooth surface of the coralline-like $ZnGa_2O_4$ sample reveals that the sample is well-crystallized [24]. This is in accordance with the analytical result of the XRD. The morphology of our sample is different from those

previously reported in the literature, i.e., rice-like [9]. Usually, a special morphology of photocatalyst benefits the photocatalytic reaction [25].

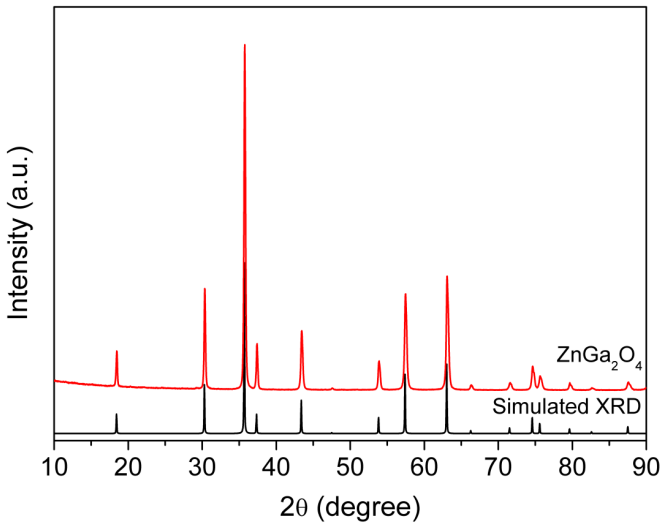

Figure 1. The powder X-ray diffraction (XRD) pattern for the $ZnGa_2O_4$.

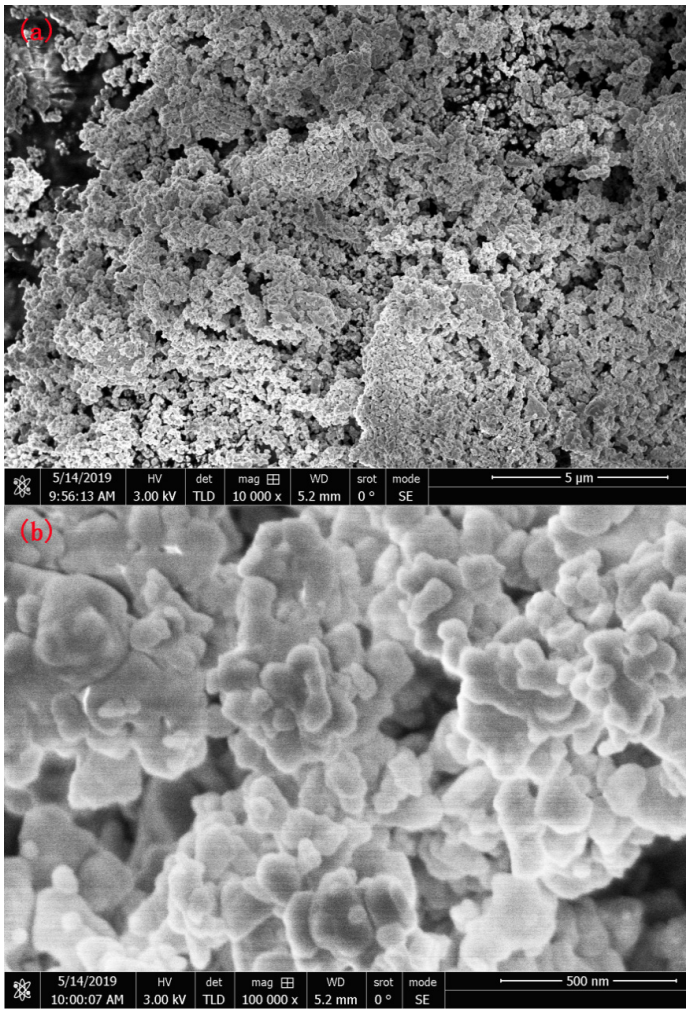

Figure 2. Scanning electron microscope (SEM) images for $ZnGa_2O_4$. (**a**) the SEM image in large-scale; (**b**) the SEM image in nano-scale.

$ZnGa_2O_4$ was then characterized by ultraviolet–visible diffused reflectance spectroscopy (UV–Vis DRS, or DRS) (see Figure 3). There is a sharp absorption peak of $ZnGa_2O_4$ located in the ultraviolet light zone, which means the as-prepared sample is an ultraviolet light responsive semiconductor. The bandgap of the $ZnGa_2O_4$ sample is calculated via this equation: $\alpha h\upsilon = A(h\upsilon - E_g)^{m/2}$, where h, υ, and A are Planck's constant, light frequency, and proportionality, respectively; m is dependent on the transition type band structure, such as a direct transition (m = 1) and an indirect transition (m = 4) [26]. The plot of $(\alpha h\upsilon)^2$ against E_g was obtained for m = 1, which suggests that the $ZnGa_2O_4$ sample is a direct transition type (see the insert image). Based on the insert image, the extrapolation method was utilized to estimate the bandgap of the $ZnGa_2O_4$ as 4.44 eV, which is close to the reported values of the bandgaps, which are in the range of 4.4–5.0 eV [27]. Usually, different morphologies of the $ZnGa_2O_4$ powder lead to different values of bandgaps.

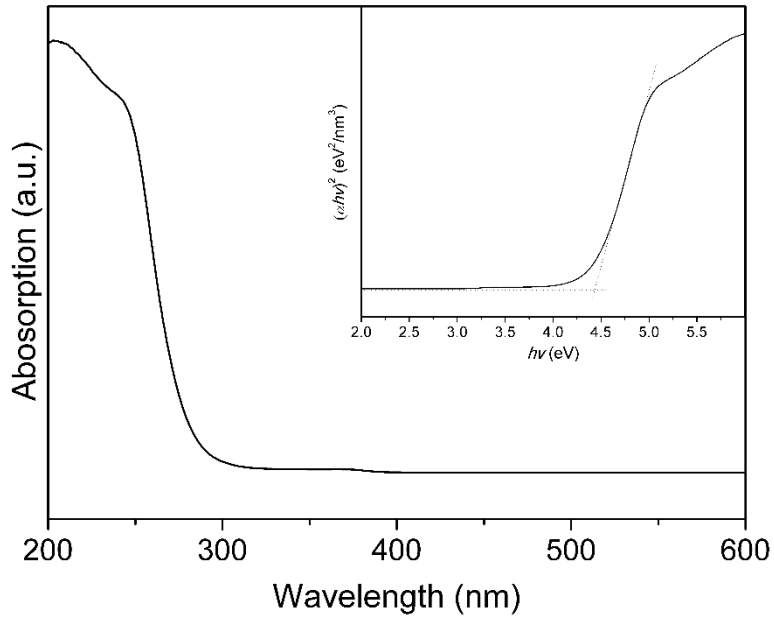

Figure 3. Ultraviolet–visible diffused reflectance spectrum (UV–Vis DRS, or DRS) for $ZnGa_2O_4$. The inset image shows the estimated bandgap energy E_g with a plot of $(\alpha h\upsilon)^2$ against photon energy ($h\upsilon$).

To study the photocatalytic activity of $ZnGa_2O_4$, 13.3 ppm RhB solution was utilized as the model wastewater in the photodecomposition reaction. Compared to the RhB solution without the photocatalyst, under irradiation with a 300 W Hg-lamp, the RhB solution with the $ZnGa_2O_4$ powder has the higher photodecomposition efficiency (see Figure S2). This indicated that the $ZnGa_2O_4$ powder acted as a photocatalyst in the photodecomposition reaction. After that, several cocatalysts were loaded on the $ZnGa_2O_4$ photocatalyst, i.e., Cu, Ag, Au, Ni, Pd, and Pt. Figure 4a displays the photocatalytic reactions for the $ZnGa_2O_4$ with 1 wt% of different cocatalysts. All of them improved the photocatalytic degradation performances of the $ZnGa_2O_4$ sample compared to the unloaded sample. To quantitatively evaluate the photodegradation activity of these samples, the reaction kinetics of the RhB photodecomposition was computed via the first-order kinetic model with $\ln(C_0/C)$ plotted against time (see Figure 4b) [28,29]. The computed k values of $ZnGa_2O_4$ with Cu, Ag, Au, Ni, Pd, and Pt cocatalysts are 0.0010, 0.0018, 0.0044, 0.0011, 0.0035, and 0.0019 min^{-1}. The k value of $ZnGa_2O_4$ with the optimal Au cocatalyst is 6.3 times greater than that of the unloaded $ZnGa_2O_4$ sample (0.0007 min^{-1}). This could be due to the strong surface plasma resonance effect of the Au cocatalyst, which increases the concentration of photogenerated electrons and thus generates hydroxyl radicals that are favorable for photodecomposition [30].

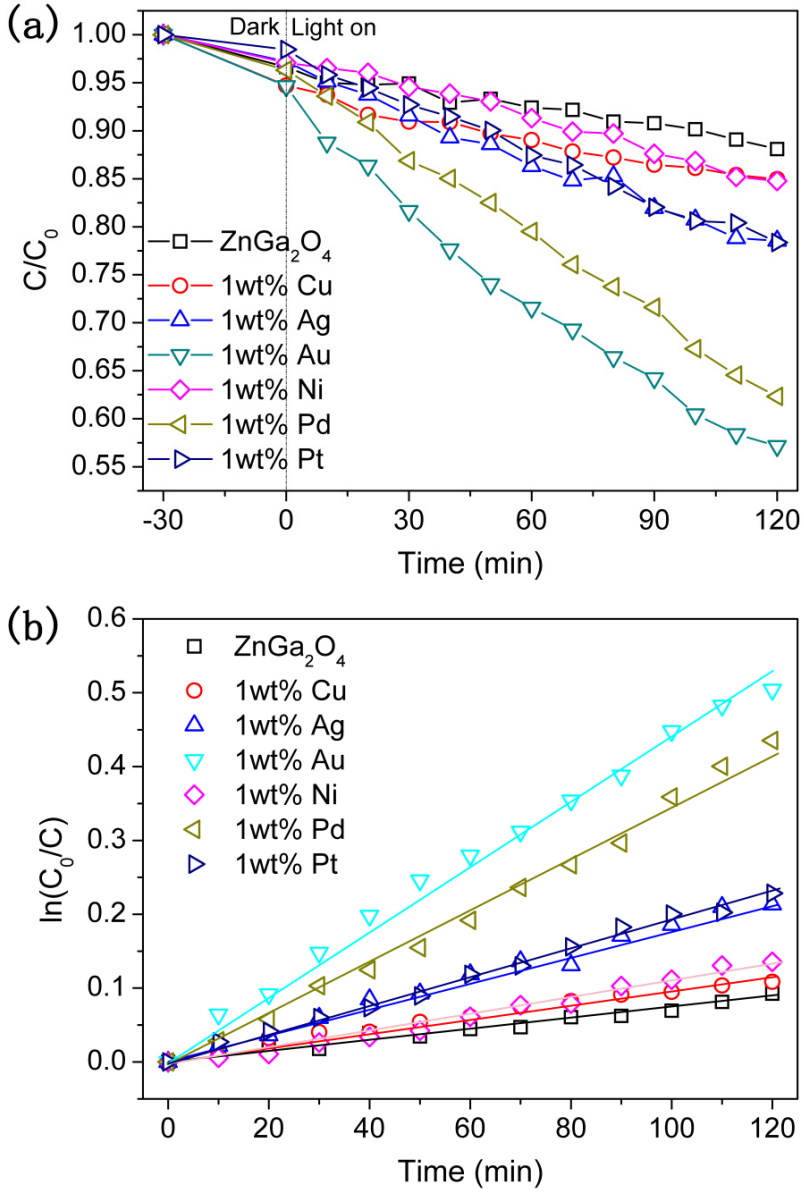

Figure 4. (**a**) The photocatalytic degradation activities of $ZnGa_2O_4$ with different cocatalysts plotted against time; (**b**) the kinetic constants of photocatalytic degradation of rhodamine B (RhB). Photocatalytic conditions were: 0.1000 g of photocatalyst, 300 mL of 13.3 ppm RhB solution, 300 W Hg-lamp.

The relationship between the $ZnGa_2O_4$ photocatalyst and the usage amount of the Au cocatalyst is displayed in Figure 5. The optimal usage amount of the Au cocatalyst is 3 wt% (see Figure S3). This could be attributed to the surface plasmon resonance effect of the Au cocatalyst [30]. Figure 5a shows the photodegradation process of the photocatalysts with different amounts of Au. The first-order kinetic model was used to calculate the k constants of these photocatalysts as well (see Figure S4). The highest k value is 0.0085 min^{-1} over $ZnGa_2O_4$ with 3 wt% Au cocatalyst. This k value is 14.1 times that of the unloaded $ZnGa_2O_4$ sample. To confirm that the relatively optimal cocatalyst is Au, the same amounts (3 wt%) of diverse cocatalysts were loaded on the photocatalyst. The kinetic constants k of these photocatalysts are 0.0038, 0.0075, 0.0085, 0.0008, 0.0020, and 0.0064 min^{-1} for the corresponding Cu, Ag, Au, Ni, Pt, and Pd cocatalysts (see Figure S5). In addition, 13.3 ppm RhB solid solutions could be completely photodecomposed over the optimal photocatalyst in 3 h (see Figure 5b). The photocatalytic degradation ratio of RhB is 96.7%.

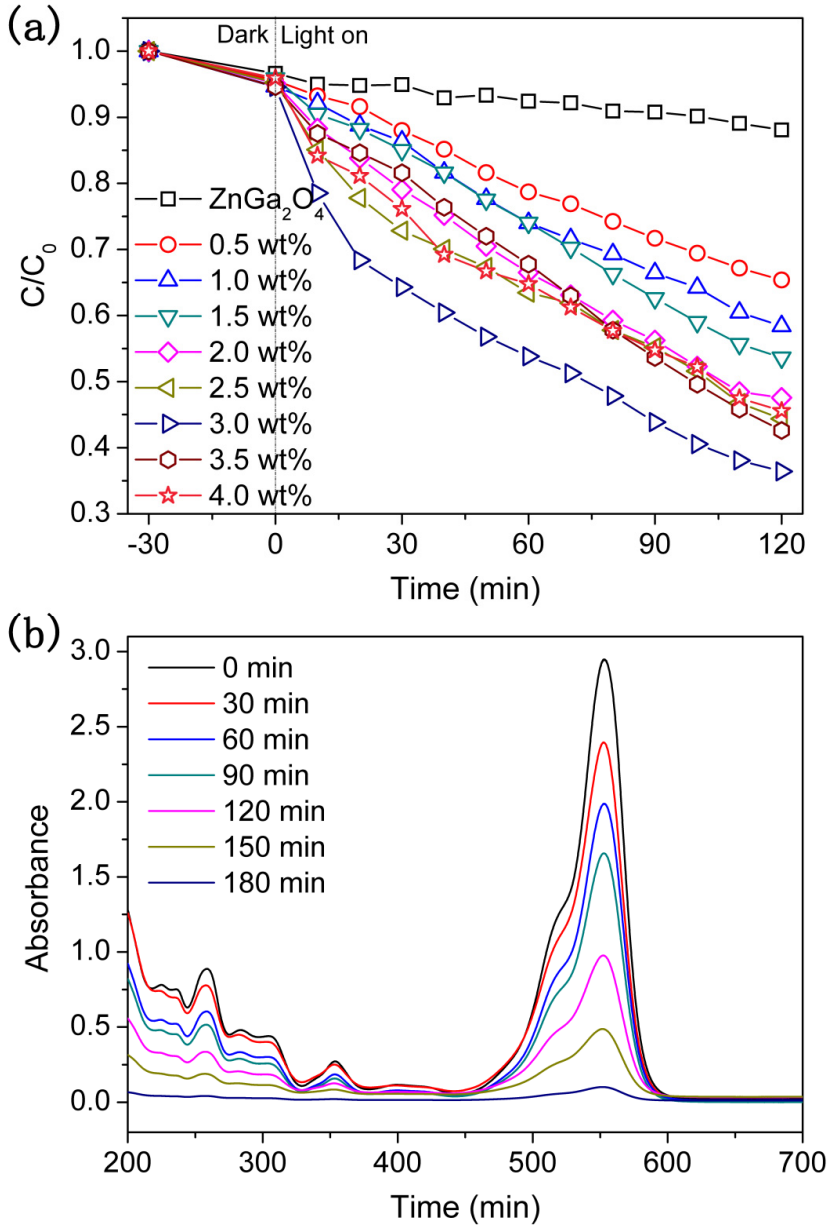

Figure 5. (**a**) The photocatalytic degradation activities of $ZnGa_2O_4$ with different amounts of the Au cocatalyst plotted against time; (**b**) The ultraviolet–visible absorption spectra of RhB at different concentrations using 3 wt% Au/$ZnGa_2O_4$ photocatalyst. Photocatalytic conditions were: 0.1000 g of photocatalyst, 300 mL of 13.3 ppm RhB solution, 300 W Hg-lamp.

To obtain further insight into the photocatalytic activity of $ZnGa_2O_4$, the electronic structure of $ZnGa_2O_4$ was computed by density functional theory (DFT). Figure 6 displays the band structure of $ZnGa_2O_4$. The theoretical bandgap (2.5 eV) is narrower than the practical bandgap from the DRS measurement. The valence band bottom and the conduction band top of $ZnGa_2O_4$ are at the same point of the band structure, which indicates that the $ZnGa_2O_4$ is a direct bandgap semiconducting material [31]. Usually, a direct bandgap semiconductor is recognized as good for the photocatalytic reaction. Besides, the top of the valence band is completely controlled by the O 2p atomic orbital, while the bottom of the conduction band is primarily composed of the hybridized orbitals of Ga 4s4p and Zn 4s4p (see Figure S6). The band structure image reveals that photogenerated carriers shift from the O 2p atomic orbital to the Ga and Zn 4s4p atomic orbitals.

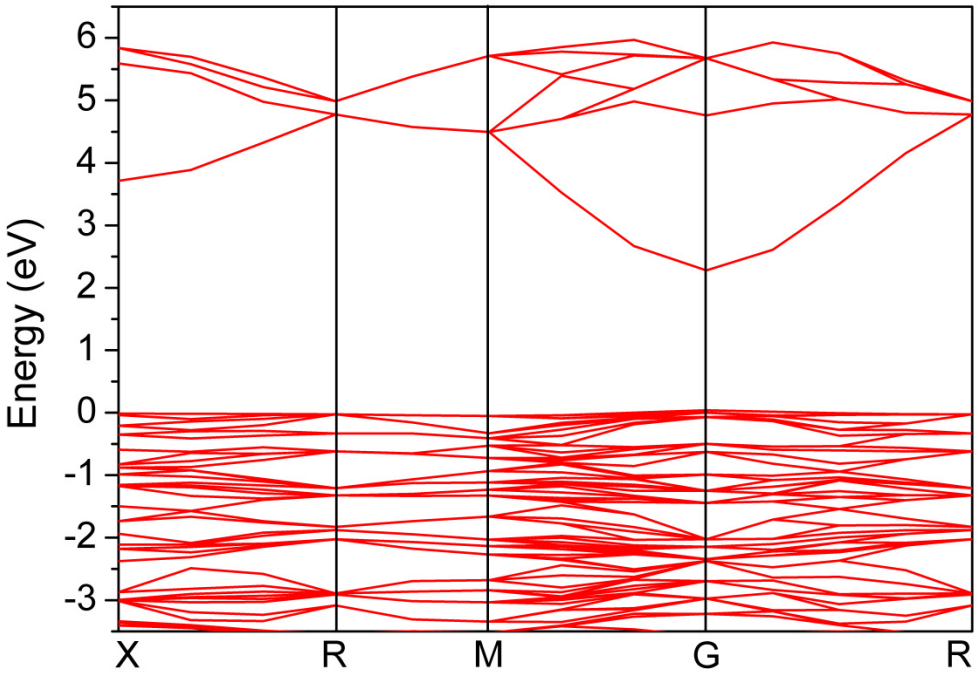

Figure 6. The electronic band structure of $ZnGa_2O_4$.

The photocatalytic mechanism of the $ZnGa_2O_4$ with the Au cocatalyst was investigated by experimental examination as well (See Figure 7). The generation of superoxide anions, holes and hydroxyl radicals was measured via the inhibition reaction with p-benzoquinone (BQ), disodium ethylenediaminetetraacetate (EDTA-2Na), and isopropanol (IPA) as respective scavengers [32,33]. Hence, we can confirm that the hydroxyl radical plays an important role in the photodegradation of RhB. However, the superoxide anion and hole play a secondary role compared to the hydroxyl radical. This is in agreement with the band structure of the $ZnGa_2O_4$, which has a wide bandgap and a high conduction band potential.

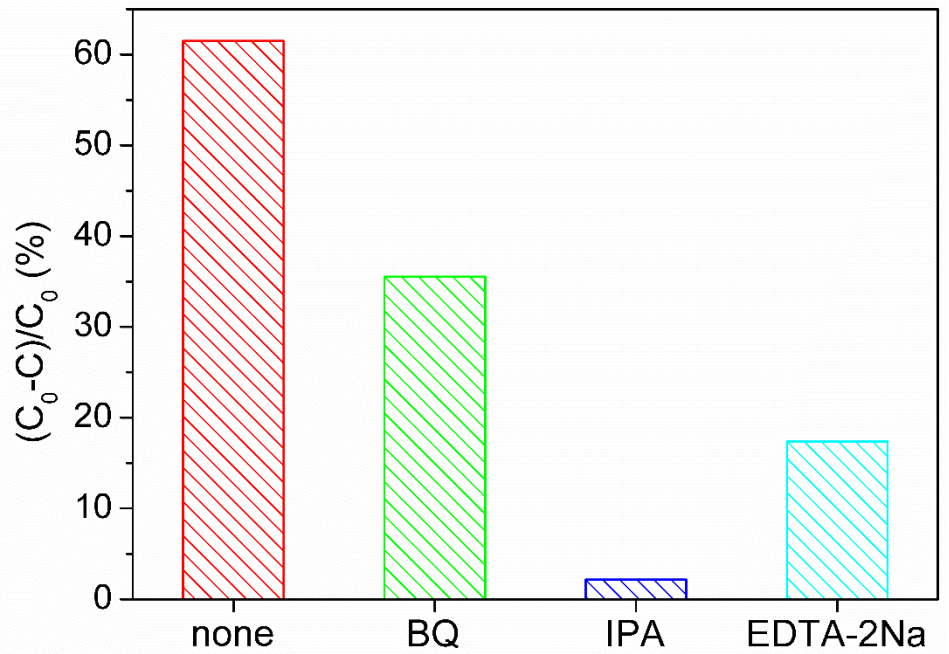

Figure 7. The photocatalytic conversion efficiency of 3 wt% $Au/ZnGa_2O_4$ for the degradation of RhB in the presence of different scavengers (1 mmol L^{-1}), under ultraviolet light irradiation.

3. Experimental Section

3.1. Preparation of the Photocatalyst

A high-temperature solid-state reaction was carried out to prepare the $ZnGa_2O_4$ sample. The starting materials, ZnO (99.9%) (Shanghai Macklin Biochemical Co., Ltd., Shanghai, China) and Ga_2O_3 (99.99%) (Adamas Reagent Co., Ltd. Shanghai, China) were directly weighed via the stoichiometric amounts of $ZnGa_2O_4$. Thereafter, the reagents were entirely homogenized and pre-heated at 600 °C for 10 h. The semi-finished powder was reground. The photocatalyst was then heated at 900 °C for another 15 h in the muffle furnace.

3.2. Characterizations of the Photocatalyst

The crystal structure of the photocatalyst was obtained via an X-ray diffractometer (PANalytical *X*'pert, Almelo, Overijssel, The Kingdom of the Netherlands), which used Cu Kα radiation. The morphology of the photocatalytst was collected via a scanning electron microscope (S-4800 SEM, Tokyo, Japan) with an accelerating voltage of 3 kV and a working distance of 5.2 mm. The bandgap of the photocatalyst was calculated via UV–Vis DRS, which was collected on a UV-3600 spectrometer (Kyoto, Japan). The incident-light intensity of the photocatalytic reaction was tested via a calibrated Si photodiode (CEL-NP2000, Beijing, China).

3.3. Calculations of Band Structure

Theoretical research on the $ZnGa_2O_4$ material was performed via the CASTEP code, which is based on standard DFT [34]. Ultrasoft pseudopotentials were employed to represent the electron–core interaction, utilizing a plane-wave set [35]. In the DFT calculations, GGA-PBE was adopted to determine the exchange-correlation potentials of the electronic structure [36]. The cutoff energy and the *k*-point were applied at 350 eV and 4×4×4, respectively.

3.4. Photocatalytic Degradation Performance Measurements

Photocatalytic degradation performances were measured on a self-assembly reaction device, which was composed of a glass reactor (300 mL, Pyre*x*) and a cold trap (quartz). The weighed photocatalyst (0.1 g) was uniformly dispersed in 250 mL of RhB solution (13.3 ppm) via a magnetic stirrer. A circulating cooling water system was simultaneously applied to keep the reaction system at a constant temperature (25 °C). A high-pressure Hg-lamp (300 W, 365 nm, CEL-LAX300, Beijing AuLight Ltd. Co., Beijing, China) was utilized to supply the light irradiation source. The intensity of the incident light was 24.7 mW/cm^2. In order to ensure adsorption–desorption equilibrium, the as-prepared $ZnGa_2O_4$ sample (0.1g) together with the RhB solution (13.3 ppm, 250 mL) were uniformly mixed in a dark room for 30 min. The ultraviolet light was applied through the cold trap, and the absorbance of the RhB aqueous solution was measured via an ultraviolet–visible spectrophotometer (UV 2600, Kyoto, Japan) at regular time intervals.

3.5. Cocatalysts

The metal cocatalyst was loaded via a photodeposition pathway utilizing the above device [37]. For instance, 0.1000 g of $ZnGa_2O_4$ photocatalyst and 6.0 mL of $AuCl_3$ (0.5 mg/mL) were homogenized in 196 mL of methanol solution (2 vol%). This mixed solution remained in the 300 mL glass reactor with ultrasonic treatment for 10 min, and thereafter the mi*x*ture was irradiated under the Hg-lamp for 1 h. The powder sample (photocatalyst with cocatalyst) was obtained for the photocatalytic degradation research. This sample was identified as Au/$ZnGa_2O_4$ 3 wt%.

3.6. Reactive Species Scavenging

The generation of superoxide anions, holes and hydroxyl radicals was measured via the inhibition reaction with BQ (0.001 M), EDTA-2Na (0.001 M), and IPA (0.001 M) as respective scavengers.

4. Conclusions

In this paper, a coralline-like $ZnGa_2O_4$ sample was prepared by a traditional high-temperature solid-state reaction. The as-prepared sample was confirmed by the powder XRD technique. The morphology of $ZnGa_2O_4$ was measured by SEM. Based on the analytical data from XRD and SEM, the $ZnGa_2O_4$ sample is a nanosized particle, 40–120 nm. The photocatalytic degradation performance of $ZnGa_2O_4$ was enhanced by cocatalysts, which were loaded via the photodeposition approach. Compared to the unloaded sample, the photodegradation efficiency of the 3 wt% Au/$ZnGa_2O_4$ photocatalyst is 14.1 times greater. The maximum photodegradation ratio of RhB for the optimal sample is 96.7% with 180 min under ultraviolet light. This simple strategy will be extended to other photocatalytic reactions.

Supplementary Materials: The following are available online at http://www.mdpi.com/2073-4344/10/2/221/s1, Figure S1: Le Bail refinements for $ZnGa_2O_4$ powder XRD patterns. The obtained cell parameters are also included. Blue circles and red lines are experimental and simulated patterns, respectively. Small blue bars below the patterns are the positions for expected reflections., Figure S2: The photocatalytic degradation RhB of $ZnGa_2O_4$ compared to blank. Photocatalytic conditions: 0.1000 g $ZnGa_2O_4$ sample, 300 mL 13.3 ppm RhB solution, 300 W Hg-lamp., Figure S3: The conversion efficiency of RhB over the $ZnGa_2O_4$ sample with different amounts of Au-cocatalyst under ultraviolet light irradiation. Photocatalytic conditions: 0.1000 g photocatalyst, 300 mL 13.3 ppm RhB solution, 300 W Hg-lamp., Figure S4: First-order kinetic constants for the photodecomposition of RhB over the $ZnGa_2O_4$ sample with different amounts of Au-cocatalyst under ultraviolet light irradiation. Photocatalytic conditions: 0.1000 g photocatalyst, 300 mL 13.3 ppm RhB solution, 300 W Hg-lamp., Figure S5: First-order kinetic constants for the photodecomposition of RhB over the $ZnGa_2O_4$ sample with 3 wt% cocatalyst under ultraviolet light irradiation. Photocatalytic conditions: 0.1000 g photocatalyst, 300 mL 13.3 ppm RhB solution, 300 W Hg-lamp., Figure S6: The electronic structure of $ZnGa_2O_4$ was calculated by a plane-wave-based density function theory.

Author Contributions: Funding acquisition, J.Y.; Investigation, W.Y. and M.Z.; Resources, J.S.; Writing—original draft, J.Y.; Writing—review & editing, X.S. All authors have read and agreed to the published version of the manuscript.

Funding: This work was financially supported by Science and Technology Project of Chongqing Municipal Education Commission (KJQN201801407) and Talent Introduction Project of Yangtze Normal University (2017KYQD22).

Acknowledgments: This work was financially supported by Science and Technology Project of Chongqing Municipal Education Commission (KJQN201801407) and Talent Introduction Project of Yangtze Normal University (2017KYQD22).

Conflicts of Interest: The authors declare no conflict of interest.

References

1. Ahmad, M.I.; Kottaisamy, M.; Rama, N.; Ramachandra, R.; Bhattacharya, S.S. Thin film luminescence of $ZnGa_2O_4$: Mn deposited by PLD. *Scr. Mater.* **2006**, *54*, 237–240. [CrossRef]
2. Cao, M.; Djerdj, I.; Antonietti, M.; Niederberger, M. Nonaqueous synthesis of colloidal $ZnGa_2O_4$ nanocrystallites and their photoluminescence properties. *Chem. Mater.* **2007**, *19*, 1239, 5830–5832.
3. Teng, Y.; Song, L.X.; Liu, W.; Xu, Z.Y.; Wang, Q.S.; Ruan, M.M. Monodispersed hierarchical $ZnGa_2O_4$ microflowers for self-powered solar-blind detection. *J. Mater. Chem. C* **2016**, *4*, 3113–3118. [CrossRef]
4. Bessiere, A.; Sharma, S.K.; Basavaraju, N.; Priolkar, K.R.; Binet, L.; Viana, B.; Bos, A.J.J.; Maldiney, T.; Richard, C.; Scherman, D.; et al. Storage of visible light for long-lasting phosphorescence in chromium-doped Zinc Gallate. *Chem. Mater.* **2014**, *26*, 1365–1373. [CrossRef]
5. Yan, S.C.; Ouyang, S.X.; Gao, J.; Yang, M.; Feng, J.Y.; Fan, X.X.; Wan, L.J.; Li, Z.S.; Ye, J.H.; Zhou, Y.; et al. A room-temperature reactive-template route to mesoporous $ZnGa_2O_4$ with improved photocatalytic activity in reduction of CO_2. *Angew. Chem. Int. Ed.* **2010**, *49*, 6400. [CrossRef] [PubMed]

6. Zeng, C.M.; Hu, T.; Hou, N.J.; Liu, S.Y.; Gao, W.L.; Cong, R.H.; Yang, T. Photocatalytic pure water splitting activities for $ZnGa_2O_4$ synthesized by various methods. *Mater. Res. Bull.* **2015**, *61*, 481–485. [CrossRef]
7. Zheng, T.T.; Xia, Y.G.; Jiao, X.L.; Wang, T.; Chen, D.R. Enhanced photocatalytic activities of single-crystalline $ZnGa_2O_4$ nanoprisms by the coexposed {111} and {110} facets. *Nanoscale* **2017**, *9*, 3206–3212. [CrossRef]
8. Zhang, Y.; Li, P.; Tang, L.Q.; Li, Y.Q.; Zhou, Y.; Liu, J.M.; Zou, Z.G. Robust, double-shelled $ZnGa_2O_4$ hollow spheres for photocatalytic reduction of CO_2 to methane. *Dalton Trans.* **2017**, *46*, 10564–10568. [CrossRef]
9. Liu, J.; Wei, L.; Wu, H.Z.; Jin, L.; Hu, B.; Li, L.L.; Wang, Z.L. In situ synthesis of rice-like $ZnGa_2O_4$ for the photocatalytic removal of organic and inorganic pollutants. *Mater. Sci. Semicond. Process.* **2016**, *56*, 251–259. [CrossRef]
10. Chen, X.; Xue, H.; Li, Z.H.; Wu, L.; Wang, X.X.; Fu, X.Z. Ternary wide band gap p-block metal semiconductor $ZnGa_2O_4$ for photocatalytic benzene degradation. *J. Phys. Chem. C* **2017**, *112*, 20393–20397. [CrossRef]
11. Tien, L.C.; Tseng, C.C.; Chen, Y.L.; Ho, C.H. Direct vapor transport synthesis of $ZnGa_2O_4$ nanowires with superior photocatalytic activity. *J. Alloy. Compd.* **2013**, *555*, 325–329. [CrossRef]
12. Wang, J.H.; Li, H.; Meng, S.G.; Zhang, L.; Fu, X.L.; Chen, S.F. One-pot hydrothermal synthesis of highly efficient SnOx/Zn_2SnO_4 composite photocatalyst for the degradation of methyl orange and gaseous benzene. *Appl. Catal. B Environ.* **2017**, *200*, 19–30. [CrossRef]
13. Li, L.; Wang, Y.H.; Li, H.; Huang, H.J.; Zhao, H. Suppression of photocatalysis and long-lasting luminescence in $ZnGa_2O_4$ by Cr^{3+} doping. *RSC Adv.* **2015**, *5*, 57193–57200. [CrossRef]
14. Sun, M.; Li, D.Z.; Zhang, W.J.; Chen, Z.X.; Huang, H.J.; Li, W.J.; He, Y.H.; Fu, X.Z. Rapid microwave hydrothermal synthesis of $ZnGa_2O_4$ with high photocatalytic activity toward aromatic compounds in air and dyes in liquid water. *J. Solid State Chem.* **2012**, *190*, 135–142. [CrossRef]
15. Zhang, W.W.; Zhang, J.Y.; Chen, Z.Y.; Wang, T.M. Photocatalytic degradation of methylene blue by $ZnGa_2O_4$ thin films. *Catal. Commun.* **2009**, *10*, 1781–1785. [CrossRef]
16. Liu, L.L.; Huang, J.F.; Cao, L.Y.; Wu, J.P.; Fei, J.; Ouyang, H.B. Synthesis of $ZnGa_2O_4$ octahedral crystallite by hydrothermal method with the aid of CTAB and its photocatalytic activity. *Mater. Lett.* **2013**, *95*, 160–163. [CrossRef]
17. Yuan, Y.F.; Huang, J.J.; Tu, W.X.; Huang, S.M. Synthesis of uniform $ZnGa_2O_4$ nanoparticles with high photocatalytic activity. *J. Alloy. Compd.* **2014**, *616*, 461–467. [CrossRef]
18. Liu, L.L.; Cao, L.Y.; Huang, J.F.; Zhang, X.W.; Wu, J.P.; Wang, K.T. Preparation and Photocatalytic Properties of the Octahedral $ZnGa_2O_4$ Crystallites. *Chin. J. Inorg. Chem.* **2012**, *28*, 2091–2096.
19. Li, X.F.; Zhang, X.Y.; Zheng, X.Z.; Shao, Y.; He, M.; Wang, P.; Fu, X.Z.; Li, D.Z. A facile preparation of $ZnGa_2O_4$ photonic crystals with enhanced light absorption and photocatalytic activity. *J. Mater. Chem. A* **2014**, *2*, 15796–15802. [CrossRef]
20. Ma, B.; Cong, R.H.; Gao, W.L.; Yang, T. Photocatalytic overall water splitting over an open-framework gallium borate loaded with various cocatalysts. *Catal. Commun.* **2015**, *71*, 17–20. [CrossRef]
21. Yang, J.; Jiang, P.F.; Yue, M.F.; Yang, D.F.; Cong, R.H.; Gao, W.L.; Yang, T. $Bi_2Ga_4O_9$: An undoped single-phase photocatalyst for overall water splitting under visible light. *J. Catal.* **2017**, *345*, 236–244. [CrossRef]
22. Zhang, L.; Liang, Q.M.; Dai, C.H.; Zhou, M.J.; Liu, Y.N. Preparation and characterization of noble metal (Pt, Ag, Ru) loaded $ZnGa_2O_4$ and its photocatalytic and photoelectric performance. *J. Mater. Sci. Mater. Electron.* **2017**, *28*, 17917–17924. [CrossRef]
23. Huang, X.; Jing, Y.; Yang, J.; Ju, J.; Cong, R.H.; Gao, W.L.; Yang, T. Flower-like nanostructure MNb_2O_6 (M = Mn, Zn) with high surface area: Hydrothermal synthesis and enhanced photocatalytic performance. *Mater. Res. Bull.* **2014**, *51*, 271–276. [CrossRef]
24. Kato, H.; Asakura, K.; Kudo, A. Highly efficient water splitting into H_2 and O_2 over lanthanum-doped $NaTaO_3$ photocatalysts with high crystallinity and surface nanostructure. *J. Am. Chem. Soc.* **2003**, *125*, 3082–3089. [CrossRef]
25. Chen, X.B.; Shen, S.H.; Guo, L.J.; Mao, S.S. Semiconductor-based Photocatalytic Hydrogen Generation. *Chem. Rev.* **2010**, *110*, 6503–6570. [CrossRef]
26. Song, K.; Yang, J.; Sun, Y.; Wang, Z.Y.; Wang, L.; Cong, R.H.; Yang, T. Improving photocatalytic water reduction activity for In_2TiO_5 by loading metal cocatalysts. *J. Alloy. Compd.* **2015**, *646*, 277–282. [CrossRef]
27. Ikarashi, K.; Sato, J.; Kobayashi, H.; Saito, N.; Inoue, Y. Photocatalysis for water decomposition by RuO_2-dispersed $ZnGa_2O_4$ with d(10) configuration. *J. Phys. Chem. B* **2002**, *106*, 9048–9053. [CrossRef]

28. Yang, H.X.; Shan, B.Q.; Zhang, L. A new composite membrane based on Keggin polyoxotungstate/poly (vinylidene fluoride) and its application in photocatalysis. *RSC Adv.* **2014**, *4*, 61226–61231. [CrossRef]
29. Yang, J.; Sun, X.R.; Zeng, C.M.; Deng, Q.H.; Hu, Y.L.; Zeng, T.; Shi, J.W. Effect of La-doped scheelite-type $SrWO_4$ for photocatalytic H_2 production. *Ionics* **2019**, *25*, 5083–5089. [CrossRef]
30. Qian, K.; Sweeny, B.C.; Johnston-Peck, A.C.; Niu, W.X.; Graham, J.O.; DuChene, J.S.; Qiu, J.J.; Wang, Y.C.; Engelhard, M.H.; Su, D.; et al. Surface plasmon-driven water reduction: Gold nanoparticle size matters. *J. Am. Chem. Soc.* **2014**, *136*, 9842–9845. [CrossRef]
31. Chen, D.; Liu, Z.; Ouyang, S.X.; Ye, J.H. Simple room-temperature mineralization method to $SrWO_4$ micro/nanostructures and their photocatalytic properties. *J. Phys. Chem. C.* **2011**, *115*, 15778–15784. [CrossRef]
32. Yang, J.; Sun, X.R.; Zeng, C.M.; Wang, X.T.; Hu, Y.L.; Zeng, T.; Shi, J.W. Highly improved photocatalytic degradation of rhodamine B over Bi_2Ga_4-$_x$$Fe_xO_9$ solid solutions under visible light irradiation. *RSC Adv.* **2019**, *9*, 2945–2949. [CrossRef]
33. Regulska, E.; Breczko, J.; Basa, A. Pristine and graphene-quantum-dots-decorated spinel nickel aluminate for water remediation from dyes and toxic pollutants. *Water* **2019**, *11*, 953. [CrossRef]
34. Segall, M.D.; Lindan, P.L.D.; Probert, M.J.; Pickard, C.J.; Hasnip, P.J.; Clark, S.J.; Payne, M.C. First-Principles Simulation: Ideas, Illustrations and the CASTEP Code. *J. Phys. Condens. Matter* **2002**, *14*, 2717–2743. [CrossRef]
35. Blochl, P.E. Projector augmented-wave method. *Phys. Rev. B* **1994**, *50*, 17953–17979. [CrossRef]
36. Perdew, J.P.; Burke, K.; Ernzerhof, M. Generalized gradient approximation made simple. *Phys. Rev. Lett.* **1996**, *77*, 3865–3868. [CrossRef]
37. Wang, G.J.; Jing, Y.; Ju, J.; Yang, D.F.; Yang, J.; Gao, W.L.; Cong, R.H.; Yang, T. $Ga4B_2O_9$: An efficient borate photocatalyst for overall water splitting without cocatalyst. *Inorg. Chem.* **2015**, *54*, 2945–2949. [CrossRef]